Journal of Applied Sciences

ISSN 1812-5654

science alert

ANSInet
an open access publisher
http://ansinet.com

Journal of Applied Sciences 10 (14): 1352-1368, 2010
ISSN 1812-5654

Plasma Wave Electronics: A Revival Towards Solid-State Terahertz Electron Devices

F. Mustafa and A.M. Hashim
Material Innovations and Nanoelectronics Research Group, Faculty of Electrical Engineering,
Universiti Teknologi Malaysia, 81310 UTM Skudai, Johor, Malaysia

Abstract: Researches on the interactions between drifting carrier plasma waves and electromagnetic waves were intensively studied theoretically and experimentally in 1960s to 1990s but faded out with inconclusive results. This study presents a series of fundamental works carried out by our group in order to re-evaluate the possibility of realizing a solid-state amplifier operating in THz region based on the drifting plasma wave interactions. Firstly, we described a new method to analyze the properties of semiconductor drifting plasma in a semiconductor-insulator structure based on the Transverse Magnetic (TM) mode analysis. The components of waves, the electromagnetic fields and the ω- and k- dependent effective permittivity which are used to describe the dielectric response of the semiconductor plasma to the TM surface wave excitation are derived. Then, the properties of semiconductor drifting plasma in a two-dimensional electron gas (2DEG) structure using the developed TM mode analysis are presented. Here, the electromagnetic fields and the ω- and k- dependent effective permittivity of the 2DEG drifting plasma are also determined. The analyzed device structure and formulation procedures to explain the interactions between drifting plasma waves in semiconductor and electromagnetic waves propagating through the interdigital slow-wave structure is then presented. Next, some preliminary experimental studies of plasma wave interactions using interdigital-gated n-AlGaAs/GaAs high-electron-mobility-structure carried out are presented. Finally, we concluded the findings or contributions of our work and some remarks for future research.

Key words: Plasma wave, HEMT, interdigital, admittance, negative conductance

INTRODUCTION

In recent years, solid-state devices operating in the so-called Terahertz (THz) gap region of electromagnetic (EM) waves are highly demanded for possible application in the field of terahertz information and telecommunication system (Chamberlain and Miles, 1997; Miles *et al*., 2001; Shur *et al*., 1999). THz gap is defined by the frequencies in the range of 0.5 ~ 10 THz. Below THz, devices classified as transit time devices and include such familiar examples as Bipolar Junction Transistors (BJTs), Heterojunction Bipolar Transistors (HBTs), Field Effect Transistors (FETs), High Electron Mobility Transistors (HEMTs) and Transferred Electron (Gunn) devices operating up to a few tens GHz are commercially available (Chamberlain and Miles, 1997; Miles *et al*., 2001; Shur *et al*., 1999). These devices are in general benefited from the advanced development of conventional electronics where reduced dimensions or sophisticated layer structures are utilized for operation beyond 100 GHz. In all of these, the time taken for carriers to move a characteristic distance determines the maximum frequency of operation. The performance of such conventional compound semiconductor devices are also compared in terms of their power amplification and operating frequency. As we know, the output powers of such conventional devices decrease with the increase of frequency where the downsizing of the characteristic distance of traditional devices is required in order to increase the operating frequency. In fact, for example, the maximum cut-off frequency obtained thus far still remains slightly above 500 GHz even with the use of very short gate length of a few nanometer and gate channel distances of a few nanometer (Watanabe *et al*., 2007). This downsizing activity does not seem to promise any merit due to not only the skyrocketing production cost but also the physical problems such as the short-channel effect and large gate leakage current. It is clear that those devices can not possess both high output power and high frequency operation where presently they are selectively used according to the required output power and operating frequency. Those devices also seem to have difficult time approaching THz range.

Above the THz gap, there are well-developed solid-state sources such as near infra-red lasers and Light

Corresponding Author: Abdul Manaf Hashim, Material Innovations and Nanoelectronics Research Group,
Faculty of Electrical Engineering, Universiti Teknologi Malaysia, 81310 UTM Skudai, Johor, Malaysia
Tel: +607-5536230 Fax: +607-5566272

Emitting Diodes (LEDs). These devices may be classified as transition devices, since the charge carriers undergo a transition from a higher to a lower energy state with the direct emission of radiation at a frequency, f given by E = hf where E is the energy state separation. It is evident that the THz gap serves to mark the boundary between electronics and photonics sources (Chamberlain and Miles, 1997; Miles *et al*., 2001; Shur *et al*., 1999).

To fill the THz gap by using conventional electron approach or transit time devices seems to be very difficult due to the limitation that comes from the carrier transit time where extremely small feature sizes are required. One way to overcome this limitation is to employ the traveling wave type approach in semiconductors like classical traveling wave tubes (TWTs) where no transit time limitation is imposed (Solymar and Ash, 1966). TWTs are well-known as an amplifier of microwave energy. It accomplishes this through the interaction of an electron beam and an EM waves propagating through a slow-wave circuit. As the electron beam travels down this interaction region, an energy exchange takes place between the electron beam and slow EM waves.

In this analogy, carriers in semiconductor correspond to the electron beam in TWTs. The interaction principle of carrier plasma waves and EM waves is thought to be in the same manner with TWTs which can lead to the amplification of EM waves. The possible mechanism of amplification can be briefly described as follows. The propagated EM waves will produce the electric fields which their directions become opposite at every half-wavelength, resulting in the acceleration and deceleration of electrons. In the case of the electron drift velocity, υ_d equals to the phase velocity of EM waves, υ_{phf} ($\upsilon_d = \upsilon_{phf}$), the amount of electrons in the acceleration region is equal to the amount of electrons in deceleration region, resulting in no energy exchange between electrons and EM waves. In the case of the electron drift velocity, υ_d slightly larger than the phase velocity of EM waves, υ_{phf} ($\upsilon_d > \upsilon_{phf}$), the bunching point of electrons will slightly shift into the deceleration region. Here, the amount of electrons in deceleration region become larger than the amount of electrons in acceleration region, resulting in the energy exchange between electrons and EM waves which leads to the amplification of EM waves. It is noted here that the behavior of these flowing electrons contribute to the so-called drifting carrier plasma wave.

Motivated by such semiconductor traveling wave amplifier concepts, there were tremendous theoretical works carried out by many researchers to evaluate the possibilities of carrier plasma wave interactions in semiconductor. The idea is to replace the electron beam in a traveling wave tube with drifting carriers in a semiconductor. These drifting charge carriers in the semiconductor would interact with the slow electromagnetic waves resulting in a convective instability. Hence, there would be the possibility of constructing a new type electromagnetic wave amplifier by injecting a signal at one end of the semiconductor and taking out an augmented signal at the other end.

Solymar and Ash (1966) published a one-dimensional analysis of an n-type semiconductor traveling wave amplifier predicting high gain per centimeter. They assumed a single species of charge carrier with infinite recombination lifetime obtaining a characteristic equation for the interaction that is reducible to the well known traveling wave tube case. This one-dimensional analysis may be valid for the coupling that takes place directly in the semiconductor bulk but in the case of using external circuit, the coupling is realized only through a surface of semiconductor which sandwiching a thin insulating layer, contacts with the slow-wave circuit. Thus, the coupling through semiconductor surface is essentially of two or three dimensions and hence, two- or three- dimensional analysis would be required for the understanding of amplification by this process.

Sumi (1967) and Sumi and Suzuki (1968) published an analysis of semiconductor traveling wave amplification by drifting carriers in a semiconductor in which he predicted 100 dB mm^{-1} gain for an InSb device operated at 4 GHz at liquid nitrogen temperature. The analysis consisted of evaluating the transverse admittance at the surface of a collision-dominant semiconductor and equating it to the transverse admittance at the surface of a developed helix (slow-wave structure). In this analysis, all the electromagnetic fields in the semiconductor are included for the estimation of propagation constants and the amplification is attained beyond the threshold that the electronic gain exceeds all the semiconductor loss. Therefore, there is no need to take into account an additional semiconductor loss. Robinson and Swartz (1967) presented an experimental evidence to claim that Sumi's assumption of no surface charges or currents at the semiconductor surface is incorrect, thus invalidating the dispersion equation so found, i.e., the equating of transverse admittance is invalid in the presence of surface current.

Zotter (1968) corrected algebraic errors in Sumi's paper and numerically evaluated the available gain for different semiconductor materials, predicting an even higher gain per millimeter. Vural and Steele (1969) have extended Sumi's analysis to consider the interaction with a generalized admittance wall including the effects of surface charge and currents. Ettenberg and Nadan (1970) published an analysis by following essentially the same

method of Solymar and Ash (1966) which applicable for two carrier species, e.g., electrons and holes and derived a maximum resistivity for a given material for which the single dominant carrier approximation remains valid. In their analysis, carrier-lattice collisions, diffusion and carrier recombination were taken into account.

Although those theories were very different but they agreed on one point, the gain may be very high (several hundred dB mm^{-1}). Motivated by the possibilities of amplification with such high gain, in particular demonstrated theoretically by Solymar and Ash (1966) and Sumi (1967) and Sumi and Suzuki (1968), some innovative experimental study was performed. Sumi and Suzuki (1968) demonstrated a coupling between drifting carriers in n-type InSb and slow electromagnetic waves in meander-type and helix-type circuits using metal-insulator-semiconductor (MIS)-structured device in the frequency range of 2-4 GHz at 77 K. Freeman *et al.* (1973) reported the electronic gains in the meander-meander line signal of up to 40 dB cm^{-1} with Ge at 4.2 K. Unfortunately, these experiments did not show any net gain and only an interaction much weaker than predicted by theory was observed. Many effects may contribute to divergence between theory and experiment. In these experiments, insulator with a few microns in thickness was used. If the thickness of insulator is made thinner, the interactions should give better results where the interactions become stronger with the reduction of distance between slow waves and carrier waves. We have shown that the magnitude of the negative conductance which is an indicator of plasma wave interaction increases with the reduction of the distance between slow-wave structure and 2DEG channel (Hashim *et al.*, 2003). Thiennot (1972a, b) also showed by using Sumi's schematic model that the thicknesses of semiconductor and insulator and electrostatic surface charge have an important effect which may cause the divergence.

Swanenburg (1973) observed the phenomena of negative conductance in the frequency range of 25-75 MHz at temperature of 25 K using n-type Si with interdigital structure. Baudrand *et al.* (1984) reported the coupling with both even and odd harmonics where large net gain of 13 dB mm^{-1} was obtained at the coupling with third harmonics in the frequency range of 1-2 GHz, using also n-type Si with interdigital structure. But, these results seem to be unreasonable due to even space harmonics do not exist in slow waves propagating through the interdigital structure. Also, in this experiment, voltage of 400-450 V was applied to accelerate carriers which this method seems to be improper for practical application.

Thompson *et al.* (1991) also claimed a gain of 13 dB mm^{-1} at 8 GHz with an applied transverse dc field of 1.5 kV cm^{-1} using n-type GaAs with interdigitated fingers and dc segmented fan antenna. In their experiments, they observed the change of reflection coefficients between the biased and unbiased states of the device which they assumed to be caused by the traveling wave interaction without any theoretical explanation.

At best only marginal internal electronic gain was observed and it was not clear that the gain mechanism corresponded to the predicted mode of operation. In contrast, in 1974 the Rayleigh (acoustic) wave amplifier, similar in principle, has achieved an external gain of 50 dB and a bandwidth of 30% (Coldren and Kno, 1974). In this case, the acoustic wave velocity is of order 10^5 cm sec^{-1}, in an easily accessible range for electron drift in semiconductor. The device was operated in the frequency range of 550-800 MHz.

Although some innovative results were demonstrated in the previous theoretical and experimental work by various group in the 1960s to 1990s, those activities faded out with inconclusive results. This is mainly due to the strongly collision-dominant nature of semiconductor plasma. Further accurate theoretical approach and proper device design supported by the remarkable progress in semiconductor materials, fabrication techniques and measurement technologies should open new hope towards the realization of solid-state THz device utilizing plasma wave interaction. In addition, the operating frequency of the devices operating based on the plasma wave interaction is related to the phase velocity of the fundamental space harmonic component which should be comparable or smaller than the electron drift velocity. Thus, pitch sizes of one hundred nanometer of slow-wave circuit like the interdigital slow-wave circuit should lead to the operation in THz region. Besides this drifting plasma concept, Dyakonov and Shur (1993) has proposed the non-drifting plasma concept and successfully demonstrated the THz detection using III-V high electron mobility transistor (HEMT). We also successfully showed the THz detection using AlGaAs/GaAs HEMT at room temperature (Hashim *et al.*, 2008). A brief analysis and discussion on the relationship between drifting plasma and such non-drifting plasma is also described in details (Mustafa and Hashim, 2010).

The objective of this study is to present a series of our fundamental works carried out since a past few years in order to re-evaluate and revive again the possibility of realizing a solid-state amplifier operating in THz region based on this drifting plasma wave interactions. In this study, a description of a new method to analyze the properties of semiconductor drifting plasma in a semiconductor-insulator structure based on the

transverse magnetic (TM) mode analysis is presented. Here, the components of waves, the electromagnetic fields and the ω- and k- dependent effective permittivity which is used to describe the dielectric response of the semiconductor plasma to the TM surface wave excitation are derived. In particular, those parameters are determined using the combination of well-known Maxwell's equations and carrier kinetic equation based on semiconductor fluid model. Following that, the properties of semiconductor drifting plasma in a two-dimensional electron gas (2DEG) structure on semi-insulating substrate using the developed TM mode analysis are presented. Here, the electromagnetic fields and the ω- and k- dependent effective permittivity of the 2DEG drifting plasma are also determined. Then, the analyzed device structure fabricated on n-AlGaAs/GaAs high-electron-mobility-transistor (HEMT) structure and the formulation procedures to explain the interactions between drifting plasma waves in semiconductor and electromagnetic waves propagating through the interdigital slow-wave structure are presented. It is noted that the approach is also applicable to other III-V compound HEMT material system. Next, the main theoretical results to show the interactions between plasma waves and electromagnetic waves are presented and their characteristics are analyzed. Here, the admittance of the interdigital-gated structure is calculated. The preliminary experimental studies of plasma wave interactions using a so-called interdigital-gated n-AlGaAs/GaAs high-electron-mobility-transistor (HEMT) structure carried out by our group are presented. Finally, we conclude the findings or contributions of our work and some remarks for future research.

TRANSVERSE MAGNETIC MODE ANALYSIS OF PLASMA WAVES IN SEMI-INFINITE SEMICONDUCTOR-INSULATOR STRUCTURE

Electromagnetic fields in semiconductor drifting plasma: The analysis is a three-dimensional analysis based on the generalization the transverse magnetic (TM) mode analysis by Sumi (1967) in such a way that the inertia effect of the electron is included. At high frequencies, a quantum mechanical treatment may become necessary. However, this is beyond the scope of the present paper. The physical situation under investigation is shown in Fig. 1.

A semiconductor plasma slab with a finite thickness d_s is separated by an insulator layer with a thickness d_I. The electromagnetic fields near the surface of an n-type semiconductor with a uniform electron flow in the z-direction with a drift velocity, υ_d, shown in Fig. 1 is

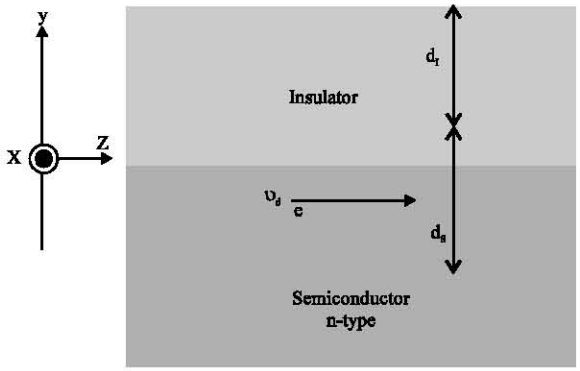

Fig. 1: Semiconductor-insulator interface and its coordinate

analyzed. The electromagnetic fields are determined by combining Maxwell's equations, the charge-current equations and the kinetic equation for electrons based on the phenomenological fluid model of the plasma given by the following equation in the effective mass approximation (Sumi, 1967; Sumi and Suzuki, 1968).

$$\left(\frac{\partial \vec{\upsilon}}{\partial t} + \vec{\upsilon}\cdot\nabla\vec{\upsilon}\right) = -\frac{q}{m^*}\left(\vec{E} + \vec{\upsilon}\times\vec{H}\right) - \frac{\upsilon_{th}^2}{n}\nabla n - \nu\vec{\upsilon} \qquad (1)$$

Here, $\vec{E}$ is the electric field, q is the electron charge, $\vec{\upsilon} = \upsilon_d$ is the electron velocity, $\vec{H}$ is the magnetic field, υ_{th} is the thermal velocity, n is the electron density, m* is the electron effective mass and ν is the collision frequency. It is shown that the plasma wave propagates in the drifting direction with a factor of exp[j(ωt-kz)] consists of two kinds of surface wave components (Hashim, 2006). One is the quasi-solenoidal wave (S-wave) without space charge perturbation (div $\vec{E}$ = 0) and the other is quasi-lamellar wave (L-wave) with space charge perturbation (rot $\vec{E}$ = 0). The transverse decay constants, Γ_s and Γ_l, of these components satisfy the following relations (Iizuka *et al.*, 2004):

$$\Gamma_s^2 = k^2 - \frac{\omega^2}{c^2} + j\frac{\omega_c(\omega - k\upsilon_d)}{c^2(\omega - k\upsilon_d - j\nu)} \qquad (2a)$$

$$\Gamma_l^2 = \frac{1}{\lambda_D^2}\left[1 - \left(\frac{\omega - k\upsilon_d}{\omega_p}\right)^2\right] + k^2 + j\frac{\nu(\omega - k\upsilon_d)}{\lambda_D^2\omega_p^2} \qquad (2b)$$

where, c is the light velocity, ω_p is the plasma frequency, and λ_D is the dielectric relaxation frequency and λ_D is the Debye length. Among ω_p, λ_D and related characteristic parameters in Eq. 2a and b, the following well-known relations hold:

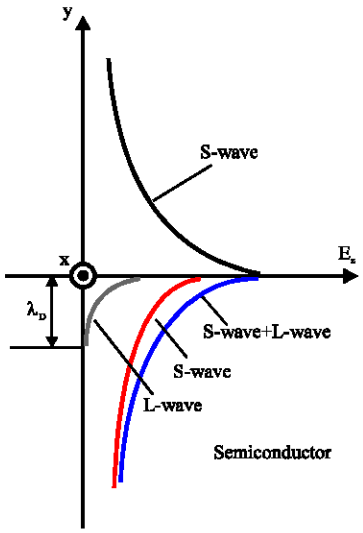

Fig. 2: S-wave and L-wave in semiconductor-insulator structure

$$\omega_p = \sqrt{\frac{q^2 n}{m^* \varepsilon}},\ \lambda_D = \sqrt{\frac{\varepsilon k_B T_e}{n q^2}} = \frac{1}{\omega_p}\sqrt{Dv} = \sqrt{\frac{D}{\omega_c}}$$
$$\omega_c = \frac{qn\mu}{\varepsilon} = \frac{q^2 n}{\varepsilon m^* v} = \frac{\omega_p^2}{v},\ D = \frac{k_B T_e}{m^* v} \quad (3)$$

where, ε is the permittivity, T_e is the electron temperature, μ is the mobility, k_B is the Boltzman constant and D is the diffusion constant.

As shown in Fig. 2 the S-wave represents the solenoidal electromagnetic field penetrating into a semiconductor whereas the L-wave represents Debye screening of fields by carriers where space charge can exist only in a surface layer with a thickness given approximately by the Debye length. In the zero temperature limits, this layer tends to a surface charge layer with zero thickness. The electromagnetic fields are obtained as follow:

$$E_y = j\frac{\Gamma_l}{k}\cdot\frac{A_l}{1 - j\frac{\omega}{k v_d}\left(\frac{v_d}{c}\right)^2} e^{\Gamma_l y} + j\frac{k}{\Gamma_s} A_s e^{\Gamma_s y} = j\frac{\Gamma_l}{k}\cdot A_l e^{\Gamma_l y} + j\frac{k}{\Gamma_s} A_s e^{\Gamma_s y} \quad (4)$$

$$E_z = A_l e^{\Gamma_l y} + A_s e^{\Gamma_s y} \quad (5)$$

$$H_x = \frac{j\omega\varepsilon}{k}\left(\frac{\Gamma_l}{k}\cdot\frac{k v_d}{\omega} A_l e^{\Gamma_l y} + \frac{k}{\Gamma_s}\left(1 - j\frac{\omega_c}{\omega}\right) A_s e^{\Gamma_s y}\right) \quad (6)$$

Here, A_l and A_s are the coefficients determined by the boundary condition at semiconductor-insulator interface. The first term and the second term of the right-hand side of Eq. 4-6 represents the quasi-lamellar component and the quasi-solenoidal component, respectively.

Boundary condition at semiconductor-insulator interface: In reality, due to various causes, the surface states will exist at the semiconductor-insulator interface. It is generally believed that the response time of the surface states is very slow, lying in the kHz to MHz region. In this analysis, the surface recombination of carriers at the semiconductor -insulator interface is ignored with the reason that the frequency range dealt in this work is high enough compared to the frequency range of surface recombination. Thus, the boundary conditions are determined as follows.

$$\varepsilon_1 E_{y1} = \varepsilon_2 E_{y2} \quad (7)$$

$$H_{x1} = H_{x2} \quad (8)$$

$$E_{z1} = E_{z2} \quad (9)$$

Here, the subscript 1 represents the insulator layer and subscript 2 represents the semiconductor layer. Using these boundary conditions, the ratio of A_l/A_s for the electric field in the z direction is obtained as follows:

$$\frac{A_l}{A_s} = j\frac{k^2}{\Gamma_s \Gamma_l}\frac{\omega_c}{\omega - k v_d} \quad (10)$$

The following Eq. 11 is obtained from Eq. 6 and 10:

$$\frac{H_{xl}}{H_{xs}} = \eta = -j\frac{k v_d \omega_c}{(\omega - j\omega_c)(\omega - k v_d)} \quad (11)$$

The above Eq. 11 shows that the s-wave component and l-wave component of electromagnetic fields have to be excited in order to be satisfied.

Effective permittivity of a semi-infinite semiconductor drifting plasma: The amplitude ratio of the above two components can be determined from the boundary condition that there can be no surface charge at finite temperatures and this leads to an expression for the ω- and k- dependent effective permittivity of the plasma, $\varepsilon_{eff}(\omega, k)$ (Iizuka *et al*., 2004; Hashim, 2006). Here, $\varepsilon_{eff}(\omega, k)$ is defined in such a way that the transverse admittance of the TM wave looking into the semiconductor plasma is given by:

$$Y = -\frac{H_x}{E_z} = \frac{i\omega\varepsilon_{eff}^{\infty}(\omega,k)}{\Gamma_s} \quad (12)$$

The TM mode analysis gives the following general expression of the effective permittivity in the slow wave approximation (|ω/k|<<c) and under assumption of an ideal semiconductor surface at the flat band condition without surface states (Iizuka *et al*., 2004; Hashim, 2006):

$$\varepsilon_{eff}^{\infty}(\omega,k)=\varepsilon_s\frac{1-\dfrac{\omega_p^{\,2}}{(\omega-kv_d)(\omega-kv_d-iv)}}{1-\dfrac{k^2}{\Gamma_s\Gamma_l}\dfrac{\omega_p^{\,2}}{(\omega-kv_d)(\omega-kv_d-iv)}} \tag{13}$$

TRANSVERSE MAGNETIC MODE ANALYSIS OF PLASMA WAVES IN SEMI-INFINITE TWO-DIMENSIONAL ELECTRON GAS STRUCTURE

Electromagnetic fields in semiconductor drifting plasma: The developed three-dimensional analysis described previously is applied to analyze the characteristics of two-dimensional electron gas (2DEG) drifting plasma at the AlGaAs/GaAs hetero-interface (Hashim *et al*., 2003; Mustafa and Hashim, 2010). In order to determine the electromagnetic fields in 2DEG semiconductor drifting plasma, the extended Transverse Magnetic (TM) mode analysis of the plasma wave interactions for the device geometry shown in Fig. 3 is performed basically following the procedures similar to those used in the previous section.

Here, we also consider that a TM wave is propagating with a uniform electron flow in the z direction, with a drift velocity, υ_d, along the 2DEG layer shown at the bottom of Fig. 3, embedded in semi-infinite GaAs and AlGaAs layers. A basic dispersion equation for TM waves can be derived by combining Maxwell's equations with the equation of electron motion in the effective mass approximation based on the fluid model of semiconductors.

The decay constants of solenoidal component, Γ_s and lamellar component, Γ_l, are obtained as follows:

$$\Gamma_s = k \tag{14a}$$

$$\Gamma_l = \frac{1}{\lambda_D} \tag{14b}$$

It was shown that only quasi-solenoidal surface wave (s-wave) components, which represent the solenoidal electromagnetic field distribution penetrating into the semiconductor region as well as that penetrating into the upper dielectric region, exist in the space and the charge modulation in the 2DEG layer can be incorporated as a boundary condition connecting these two s-wave components, i.e., one in the lower semiconductor

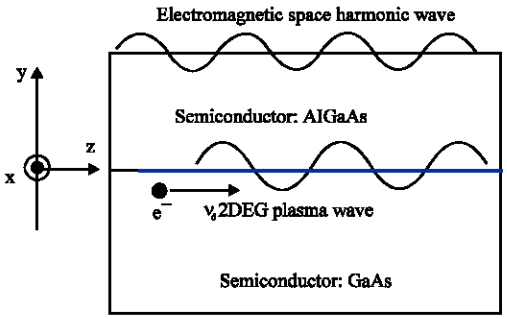

Fig. 3: 2DEG AlGaAs/GaAs heterointerface and its coordinate

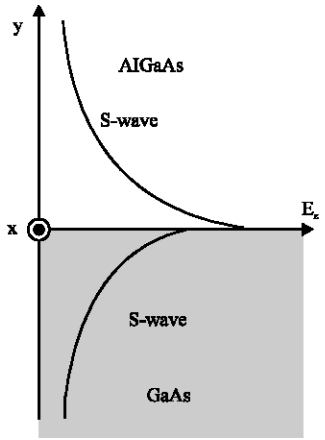

Fig. 4: S-wave in AlGaAs/GaAs structure

half-space and the other in the upper dielectric half-space, these two s-wave components are schematically shown in Fig. 4.

The effect of lamellar component is very small due to the confinement of carriers in 2DEG layer. Using the 2DEG layer, the loss due to the transverse carrier diffusion of the s-wave can be suppressed due to strong quantum confinement. The s-wave component of E_y, E_z and H_x are summarized as follows (Hashim, 2006; Mustafa and Hashim, 2010).

$$E_{sy} = Y_s\frac{k}{\omega\varepsilon^*}\left(A_s^+e^{\Gamma_s y}-A_s^-e^{-\Gamma_s y}\right) \tag{15}$$

$$E_{sz} = A_s^+e^{\Gamma_s y}+A_s^-e^{-\Gamma_s y} \tag{16}$$

$$H_{sx} = -Y_s\left(A_s^+e^{\Gamma_s y}-A_s^-e^{-\Gamma_s y}\right) \tag{17}$$

where, A_s^+ and A_s^- are the coefficients determined from the boundary condition.

Effective permittivity of drifting plasma in 2DEG on semi-insulating substrate: Similarly, from the TM wave analysis of the 2DEG layer, the admittance of plasma for 2DEG is defined (Hashim, 2006; Mustafa and Hashim, 2010) as:

$$Y = -\left.\frac{H_x}{E_z}\right|_{2DEGsurface} = \frac{i\omega\varepsilon_{eff}^{\infty}(\omega,k)}{\Gamma_s} \quad (18)$$

where, the ω- and k- dependent effective permittivity of the 2DEG plasma was calculated as:

$$\varepsilon_{eff} = \varepsilon_{GaAs}\left[1-\left(\frac{q^2 n_S}{m^*\varepsilon_{AlGaAs}}\right)\frac{k}{(\omega-k\upsilon_d)(\omega-k\upsilon_d-jv)}\right. \quad (19)$$
$$\left.\times\frac{1}{1-\frac{(k\upsilon_{th})^2}{(\omega-k\upsilon_d)(\omega-k\upsilon_d-jv)}}\right]$$

THEORETICAL ANALYSIS OF INTERACTION BETWEEN PLASMA WAVES AND ELECTROMAGNETIC SPACE HARMONIC WAVES

Device structure and theoretical formulation: A theoretical analysis procedure to describe the presence of interactions between surface plasma waves of carriers in a 2DEG at AlGaAs/GaAs heterostructure and electromagnetic space harmonics slow waves using interdigital-gated HEMT plasma wave devices are presented, the schematic physical device structure is shown in Fig. 5.

The carrier plasma waves are assumed to propagate along the 2DEG layer with the phase factor of exp(j(ωt-kz)) in the z direction as shown at the bottom of Fig. 5. The effective permittivity derived in the previous section was utilized in the calculation of the two-terminal admittance of the interdigital structure shown in Fig. 5. With reference to Fig. 6, a periodic Green's function, Gr(z, z'), for the multiconductor strip lines (Hasegawa *et al*., 1971; Silvester, 1968) was defined as the potential at point z on a metal finger in response to an array of the unit positive and negative charge lines placed at positions of z' + mp with m = 0, ±1, ±3, ±5,….. Then, Gr(z, z') was calculated as follows (Hashim *et al*., 2003; Mustafa and Hashim, 2010):

$$Gr(z,z') = \sum_{\substack{n=-\infty \\ odd}}^{\infty}\frac{\exp^{-ik_n(z-z')}}{|k_n|p(\varepsilon_o+\varepsilon_{eff}^{*}(\omega_n,k_n))};\ k_n = \frac{\pi}{p}n(n=\pm1,\pm3,\pm5,.....) \quad (20)$$

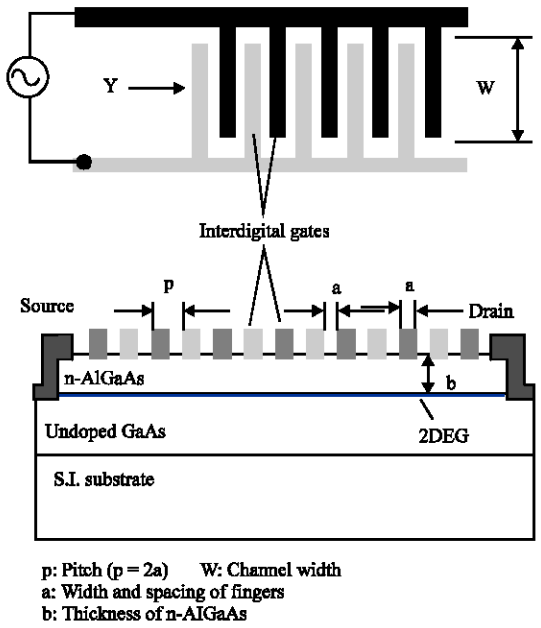

Fig. 5: Physical device structure under study

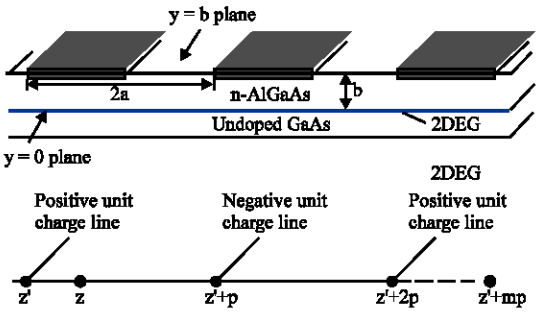

Fig. 6: Schematic for admittance analysis of interdigital gates

where, ε_0 is the permitivity of vacuum and ε_{eff}^{*} is the effective permitivity of the 2DEG plasma.The interdigital admittance was evaluated by solving the following Fredholm's integral equation on a computer using matrix algebra (Seki and Hasegawa, 1984) in order to obtain the charge distribution, ρ(z), on the finger, where Φ_0 is the potential of the finger.

$$\Phi_0 = \int_{finger} Gr(z,z')\rho(z')dz' \quad (21)$$

Finally, the interdigital two-terminal admittance was evaluated by the following equation:

$$Y = G + j\omega C = \frac{1}{\Phi_0}\int_{finger}\rho(z)dz \quad (22)$$

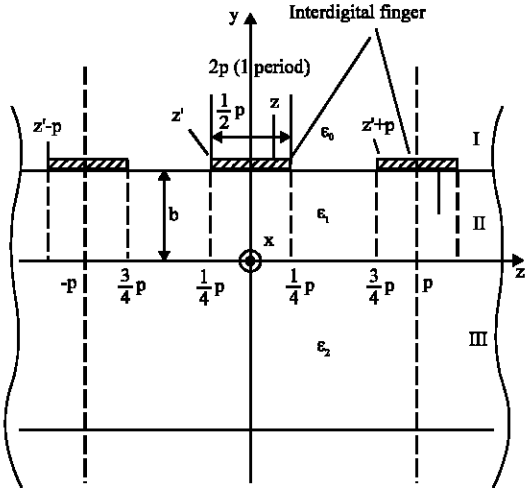

Fig. 7: Schematic for space harmonic analysis of interdigital

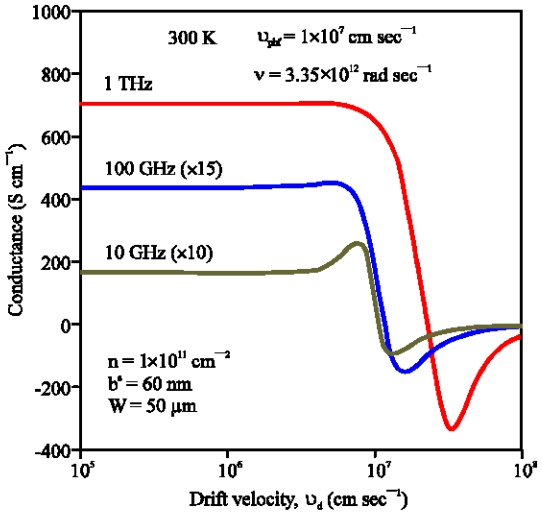

Fig. 8: Calculated conductance as a function of drift velocity for 10 GHz, 100 GHz and 1 THz

where, G and C are the conductance and capacitance of the interdigital structure loaded with 2DEG plasma, respectively.

Space harmonics in interdigital slow-wave structure: The basic characteristics of the interdigital slow-wave structure were theoretically considered in terms of the existence of space harmonics in this structure. The cross-sectional structure for consideration is shown in Fig. 7 (Hashim, 2006; Hashim *et al*., 2007a, b). This structure is divided into three regions as follows:

Region I ($b \le y < +\infty$): dielectric layer with dielectric permittivity constant, ε_0.
Region II ($0 \le y < b$): dielectric layer with dielectric permittivity constant, ε_1.
Region III ($-\infty \le y < 0$): semiconductor layer with dielectric permittivity constant, ε_2.

The channel of carrier flow is assumed to be at the plane of y = 0 and the interdigital slow-wave structure is assumed to be located at the plane of y = b where its thickness is ignored (infinitely thin) and has a unit length in x direction. As shown in Fig. 7, these interdigital fingers are arranged in z direction. The difference of phase angle between two adjacent fingers is assumed to be equal to π. In this analysis, we found that only odd space harmonics propagates in the interdigital slow-wave structure.

Appearance of negative conductance: Using the procedure mentioned previously, the two-terminal interdigital admittance of the present device was calculated numerically on a computer. Calculation was carried out for wide range of parameters and negative conductance was obtained in various cases (Hashim *et al*., 2003). It was found that large negative conductance values can be obtained under a condition when the drift velocity slightly exceeds the phase velocity, υ_{phf} = f (frequency) x 2p, of the fundamental space harmonic component of electromagnetic wave.

Examples of calculated conductance are plotted as a function of drift velocity for 10, 100 GHz and 1 THz at 300 K in Fig. 8 for the case of $\upsilon_{phf} = 1\times10^7$ cm sec^{-1}, $n_{so} = 1\times10^{11}$ cm^{-2} and the AlGaAs thickness, b = 60 nm. Here, the occurrence of negative conductance peak is seen when the electron drift velocity slightly exceeds phase velocity, υ_{phf}. Since the value of pitch, p, reduces with the increase of frequency for the same value of phase velocity, υ_{phf}, the available value of negative conductance per area is predicted to be very large, being of the order of 300 S cm^{-1} at 1 THz for $\upsilon_{phf} = 1\times10^7$ cm sec^{-1}, $n_{so} = 1\times10^{11}$ cm^{-2} and b = 60 nm.

EXPERIMENTAL STUDY OF PLASMA WAVE INTERACTIONS USING INTERDIGITAL-GATED HEMT STRUCTURES

Device structure and measurement method: A preliminary experimental study on the presence of interactions between surface plasma waves of carriers in a 2DEG at AlGaAs/GaAs heterostructure and electromagnetic space harmonics slow waves using interdigital-gated HEMT plasma wave devices are presented by Hashim *et al*. (2005, 2007a, b). A mesa pattern was formed on the MBE-grown AlGaAs/GaAs

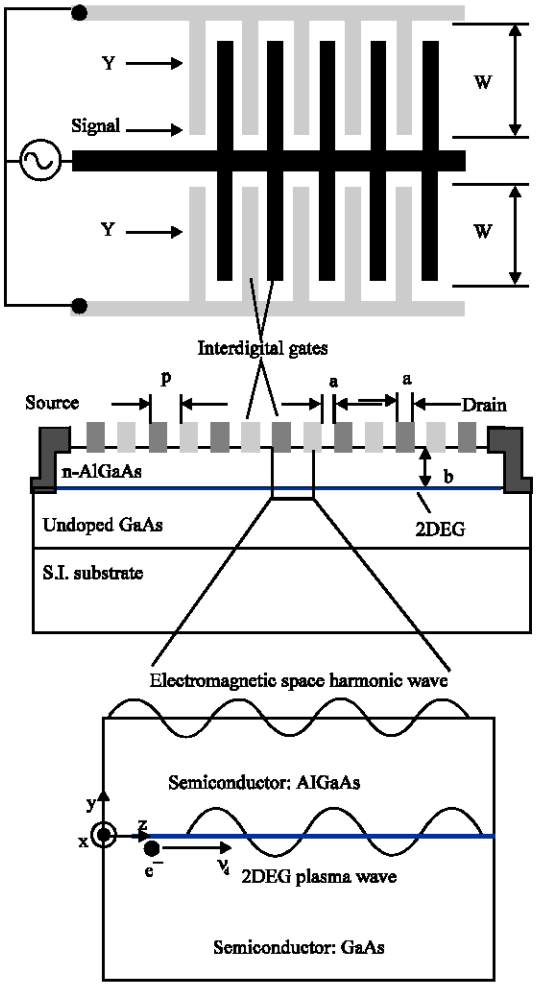

Fig. 9: Physical device structure of AlGaAs/GaAs interdigital-gated HEMT device with dc connected fingers

sample using electron beam lithography (EBL). The etchant used (H_2SO_4 : H_2O_2 : H_2O with a ratio of 8:1:1) produces anisotropic edge profiles. Then, the ohmic contact patterns are formed by photolithography or EBL and Ge/Au/Ni/Au metals were deposited using vacuum deposition method. After that, Schottky interdigital gate patterns are formed by EBL and then Cr/Au metals are deposited using the same deposition method.

A fabricated device with dc connected interdigital finger structure is schematically shown in Fig. 9. This device is similar to conventional HEMT in which a set of interdigital electrodes act as Schottky gate. However, the use of the device is very different. We are interested in the two-terminal admittance of the interdigital gate itself, which should be strongly modulated and which even becomes negative in its real part due to the wave interactions between plasma waves and electromagnetic space harmonic waves. As shown at the top of Fig. 9, the interdigital slow-wave circuits consist of two comb-like electrodes and have 25 pairs of fingers/channel with a finger pitch, p, of 5 or 10 μm. Here, the finger width and spacing are chosen to be the same and equal to a, so that p is equal to 2a. In the present device design, two channels were formed.

The device has the overall structure of a loaded coplanar waveguide (CPW), which facilitates on-chip microwave probing. The channel width, W, was 50 μm and the thickness of the AlGaAs barrier layer was 50 nm. The carrier mobility and the carrier sheet density obtained by Hall measurements at room temperature are 7540 cm^2/Vs and 4.6×10^{11} cm^{-2}, respectively. A plan view of the fabricated device is shown in Fig. 10.

The two-terminal admittance, Y, of the plasma wave device was determined from the S-parameter reflection measurement, as shown in Fig. 10 over the frequency range from 1 to 15 GHz at room temperature using a vector network analyzer HP8510C and a Cascade on-wafer microwave microprober of Ground-Signal-Ground type. It was shown theoretically in the previous section that traveling-wave interaction becomes more and more favorable at higher frequencies, particularly in the THz region. However, direct measurement of two-terminal admittance at such ultra-high frequencies is very difficult. Therefore, the measurements are carried out only at low microwave frequencies. During the measurement, the source and drain were biased with dc voltage, V_S and V_D, respectively to cause drift current to flow in the channel while the dc voltage to the set of interdigital fingers was kept at zero.

Large conductance modulation and comparison with theory: The measured admittance of the two-terminal interdigital structure are summarized in Fig. 11a and b as a function of the drain-source voltage, V_{DS}, for a device with a pitch of 5 μm under zero gate voltage for all the interdigital fingers (Hashim *et al*., 2005, 2007a, b). The measured values of conductance and capacitance experience remarkably large changes with changes of the drain-source voltage for all the measured frequencies. The conductance decreases rapidly at 5 and 10 GHz when the drain-source voltage slightly exceeds 4V. Obviously, the observed behavior of the admittance of the interdigital gates cannot be explained at all by the conventional transport theory with the transit time picture. These results indicate the presence of the effect of the interactions between the surface plasma waves of 2DEG carriers and electromagnetic space harmonic waves in the fabricated interdigital-gated HEMT device.

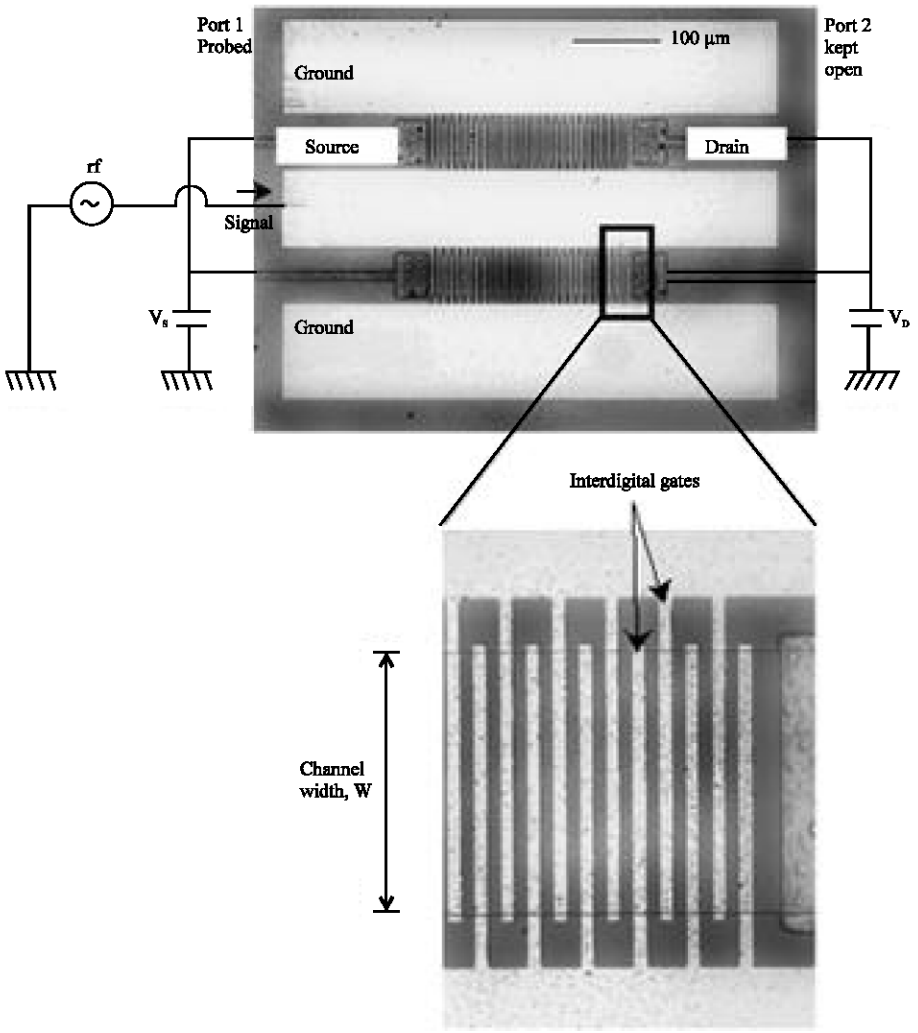

Fig. 10: Plan-view of fabricated AlGaAs/GaAs interdigital-gated HEMT device with dc connected fingers

However, a suitable theoretical analysis is required to confirm the presence of such an effect quantitatively. The calculation results of interdigital admittance based on our theoretical approach explained previously are shown in Fig. 12a and b. The calculated values of conductance and capacitance also experience remarkably large changes with changes of the drain-source voltage for all the calculated frequencies. Here, small values of negative conductance are obtained.

Effect of field non-uniformity along the channel: Theoretical curves in Fig. 12a and b show that drastic variations in conductance and capacitance take place with the drain-source voltage over all frequencies. The calculated values of conductance and capacitance have nearly the same magnitudes as the experimental ones (Hashim *et al*., 2005, 2007a, b). Thus, the general behavior of the admittance is reproduced surprisingly well by calculation in spite of various assumptions used in the theory. The major assumptions in the theory are: (1) the interdigital pattern is infinitely repeated; (2) the thickness of the electrode pattern is infinitely thin, but its conductance is infinitely large; (3) the phase of the electromagnetic field on the metal is maintained the same in the finger direction (x-direction) for all frequency components and (4) the carriers have the same drift velocity along the whole channel.

In spite of the above general remarks, however, agreements on the details are obviously not adequate between theory and experiment. Particularly, the appearance of a small negative conductance is predicted

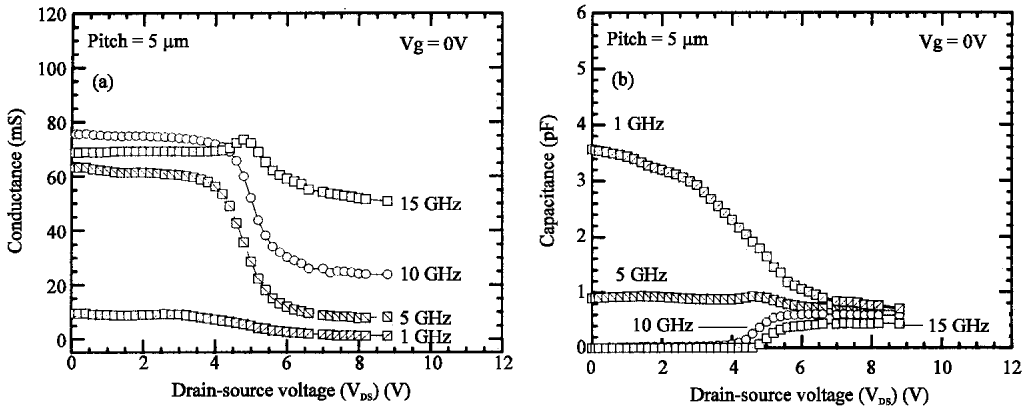

Fig. 11: Measured (a) conductance and (b) capacitance characteristics as a function of drain-source voltage

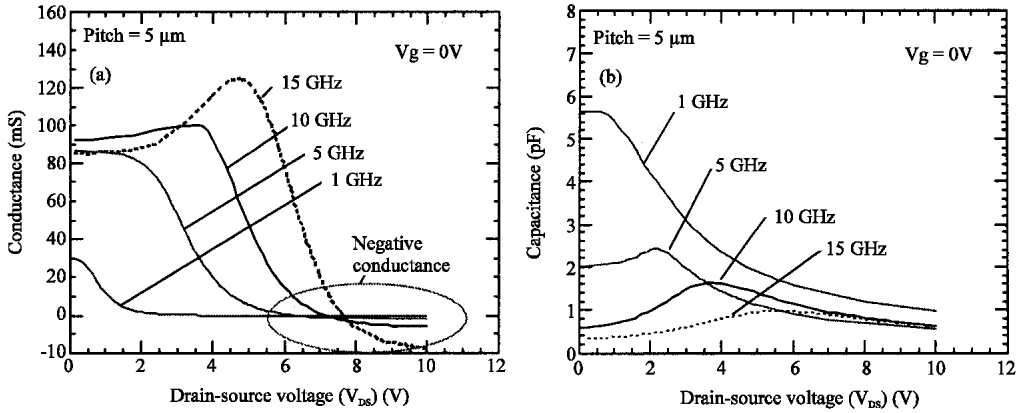

Fig. 12: Calculated (a) conductance and (b) capacitance characteristics as a function of drain-source voltage

by theory at drain-source voltages above 7.5 V for frequencies ranging from 10 to 15 GHz and this behavior was, unfortunately, not seen in the experiment.

We believe that the major cause for the lack of agreement in the detailed behavior comes from assumption (4) in which the carriers have the same drift velocity along the whole channel. This is not the case in any semiconductor field-effect transistor under a strong drain bias. The nonoccurrence of negative conductance in the experiment can be explained in terms of cancellation of the small negative conductance obtained under the high field portion of the channel by the large positive conductance coming from the low field portion of the channel.

To take account of this effect, we have estimated the electric field distribution, E(z) under the interdigital gates by fitting the dc drain I-V characteristics using the gradual channel approximation and the field-dependent mobility. Here, we replace the entire interdigital pattern with one gate electrode, since the surface potential of the air-gap region is similar to that underneath the gate with zero-bias due to strong Fermi level pinning. From the estimated field distribution, we obtained the drift velocity under each interdigital finger, v_d^{finger}, using the following equation:

$$v_d^{finger} = \frac{\mu_0 E(z)^{finger}}{1 + \frac{\mu_0}{v_s} E(z)^{finger}} \quad (23)$$

where μ_0 is the low-field mobility and v_s is the saturation velocity. Then, the interdigital admittance is calculated by

$$Y = \sum_{finger} (G^{finger} + iB^{finger}) \quad (24)$$

where, G^{finger} and B^{finger} are the conductance and susceptance of the individual interdigital fingers, respectively. For the values of G^{finger} and B^{finger}, we used the values assuming uniform velocity distribution, taking advantage of gradual changes in velocity along the channel and the quasi-periodic nature of the interdigital pattern.

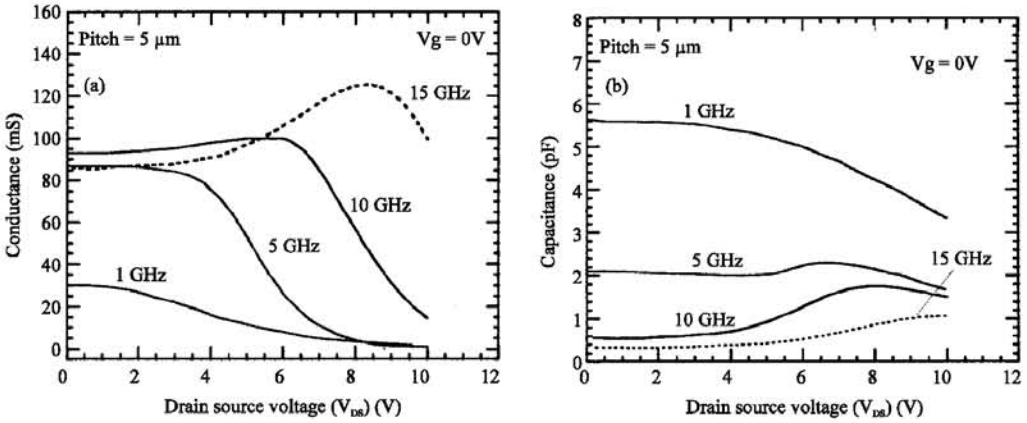

Fig. 13: Calculated (a) conductance and (b) capacitance characteristics as a function of drain-source voltage taking into account the uniformity of field distribution along the HEMT channel

The recalculated conductance and capacitance, taking into account the non- uniformity of the field in this fashion, are shown in Fig. 13a and b, respectively. The recalculated results show much better agreements with the experimental ones shown in Fig. 11a and b in spite of a very simple theoretical treatment of a very complicated problem. Thus, it can be concluded that the observed changes in both conductance and capacitance are due to the coupling between the drift plasma waves in the 2DEG carriers and the electromagnetic space harmonic slow waves through the interdigital pattern.

Behavior of capacitively coupled device: We believe that uniform carrier drift velocity should be realized if the potential array is arranged in the same slope or in the step-like distribution (Hashim, 2006; Hashim *et al.*, 2007a, b). Ideally, such a potential distribution can be realized by introducing a different individual bias to each finger. However, this method is totally not suitable for real application. Here, we come with the idea that the most possible way is to make all fingers being capacitively coupled. This structure also called as dc segmented rf coupled structure. This structure will keep uniform electric field in the channel when the dc bias is applied to the interdigital gates which modulates the potential in the channel.

The schematic structure of fabricated device with capacitively coupled fingers is shown in Fig. 14. The structure of interdigital fingers on the channel area is not changed which is similar to a dc connected structure shown in Fig. 9. The plan view of the fabricated device is shown in Fig. 15. The fingers are capacitively coupled through SiO_2 layer (thickness = 300 nm) only at certain part as indicated in Fig. 15. SiO_2 layer on the channel was etched out. The other device parameters such as pitch

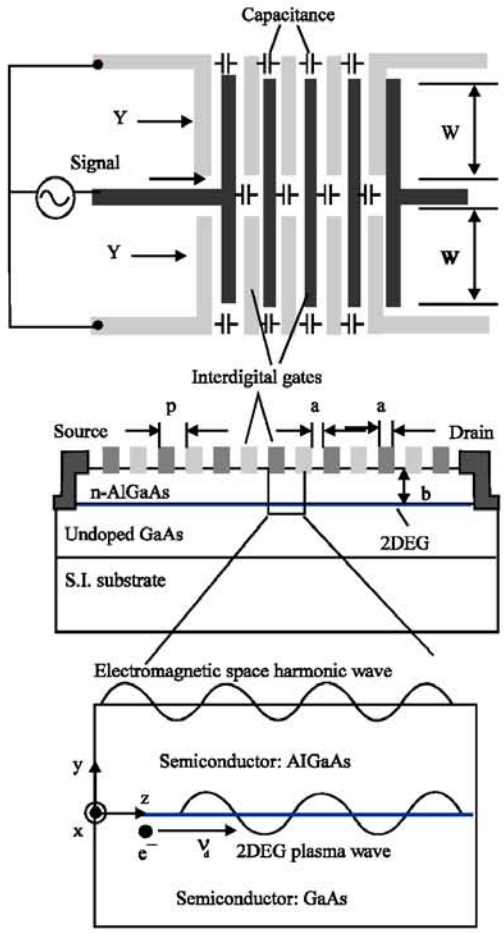

Fig. 14: Schematic device structure with capacitively coupled interdigital fingers

size, number of fingers, carrier mobility and carrier sheet density are same with the previous dc connected

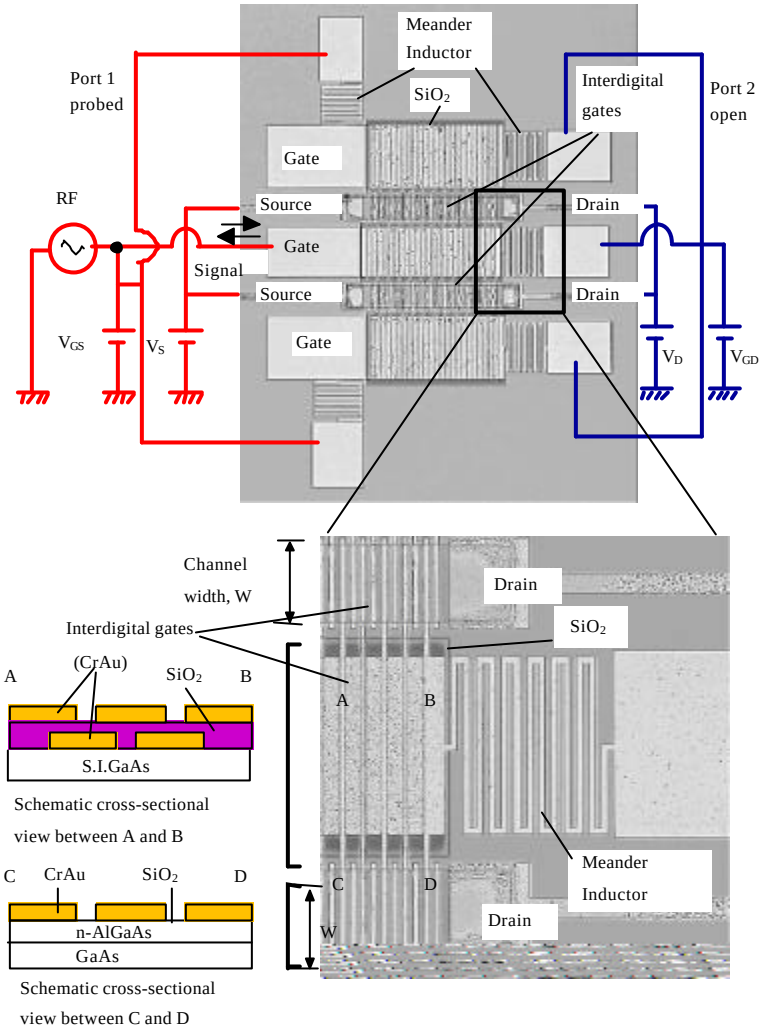

Fig. 15: Plan-view of fabricated device with capacitively coupled interdigital fingers

structure. Only the channel width was designed to be 40 μm. In addition, five meander-type inductors with the width of 3 μm were applied to block the rf signal from going through to the dc probe. It was confirmed that the rf leakage is less than 1%.

The measurements were also carried out at low microwave frequencies in the range of 10 to 40 GHz and their setups were also shown schematically in Fig. 15. During the measurement, as shown in Fig. 15, the source and drain were biased with dc voltage, V_S and V_D respectively to cause drift current to flow in the channel while the dc voltages to the set of interdigital gates, V_{GS} and V_{GD}, were adjusted to a desired gate voltage, V_G according to the following group of Eq. 25:

$$V_S = \frac{-V_{DS}}{2};\ V_D = \frac{V_{DS}}{2};\ V_{GS} = V_G + V_S = V_G - \frac{V_{DS}}{2};\ V_{GD} = V_G + V_D = V_G + \frac{V_{DS}}{2} \quad (25)$$

By isolating fingers by capacitors and by using meander inductors, such a special dc biasing described above is realized so as to achieve a uniform field distribution along a channel assumed in theory, since conventional HEMTs produce a highly nonuniform field distribution in the channel. In addition, this structure allows the adjustment of the gate voltage which was not realized using previous dc connected structure.

The measured dc I-V characteristics of a device measured by this special biasing method, as shown in Fig. 16 shows the shift of pinch off voltage and extension of linear region as compared with conventional FET gate operation shown in Fig. 17. Thus, it can simply confirm that uniformity of field distribution was improved. Here, the calculation results for both cases were carried using the following equation:

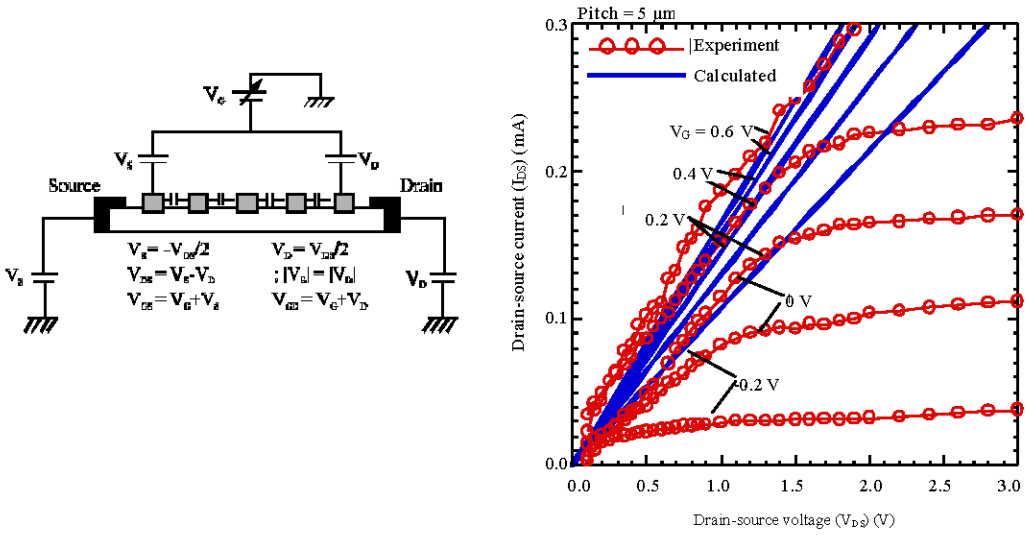

Fig. 16: dc I-V characteristics measured by special biasing method

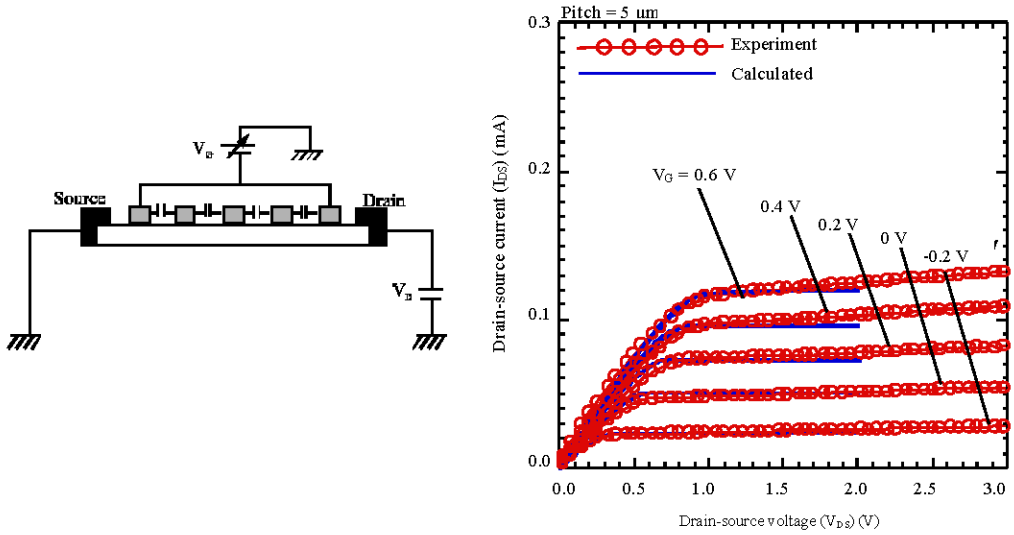

Fig. 17: dc I-V characteristics measured by conventional FET method

$$I_{DS} = \frac{\mu W_G \varepsilon_{AlGaAs}}{L_G b}\left\{(V_G - V_T)V_{DS} - \frac{1}{2}\left(V_D^2 - V_S^2\right)\right\} \qquad (26)$$

where, W_G is the channel width, L_G is the gate length, I_{DS} is the drain-source current and V_T is the threshold voltage. It is indicated in Fig. 16 that the calculated results for special biasing method show no pinch off behavior as what seen in the experimental ones. It is noted here, for the special bias method the second term in the bracket of Eq. 26 is zero. This discrepancy is believed due to the fingers at the both edges as shown in Fig. 14, were made directly connecting of to the main gate electrodes where these fingers have pinched off the channel. By making all the fingers not only being capacitively coupled among each other but also to the main gate electrodes, the pinch off of the channel should be prevented. This design will be carried out in the future work.

The measured conductance is shown as a function of drain-source voltage, V_{DS} for various gate voltages in Fig. 18a and for various frequencies in Fig. 18b, respectively (Hashim *et al.*, 2007a, b). The change of conductance using this structure takes place at low V_{DS} as compared with dc connected interdigital finger structure. Thus, it can be assumed that uniformity of field

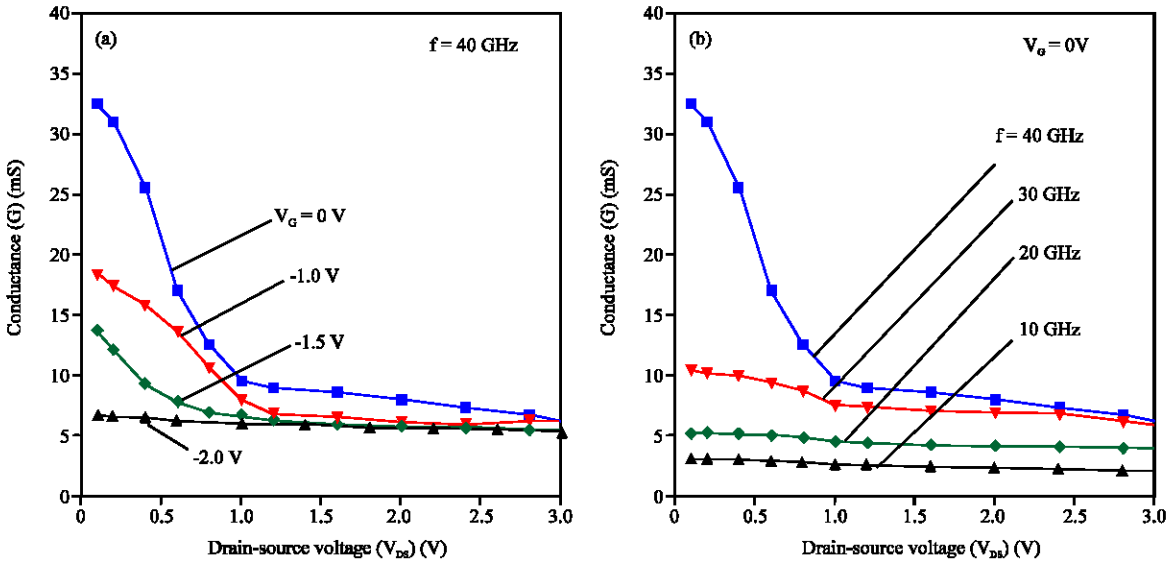

Fig. 18: Measured conductance as a function of drain-source voltage (a) gate voltage dependence and (b) frequency dependence

distribution was improved. The dc I-V measurements indicated that ample carriers are in the channel at zero gate bias which totally pinches off at -2V. Conductance modulation by V_{DS} for channels with ample carriers could be clearly seen and this absolutely only can be explained in terms of interactions between the input rf signals and 2DEG surface plasma waves. Absolute conductance values were smaller than the theoretical prediction, due to the small capacitance between interdigital fingers attenuating the propagation of rf signal at these frequencies.

CONCLUSIONS

A new method based on the Transverse Magnetic (TM) mode analysis for analyzing plasma wave interactions in semiconductor-insulator structure and semiconductor with 2DEG structure was presented. In this analysis, two kinds of excited wave components were shown to exist in the semiconductor-insulator structure which are known as quasi-lamellar wave (l-wave) and quasi-solenoidal wave (s-wave). On the other hand, the excited surface wave component in 2DEG semiconductor was shown to be only dominated by quasi-solenoidal wave which should improve the interactions between carrier plasma waves and electromagnetic waves. The effective permittivity which is used to describe the dielectric response of the semiconductor plasma to the TM surface wave excitation was derived for both structures. It was shown that only the odd mode of space harmonics propagate through the interdigital slow-wave structure. An occurrence of negative conductance was predicted when the drift velocity of carriers slightly exceed the phase velocity of electromagnetic space harmonic slow waves. Although the magnitude of negative conductance peak is small at low microwave frequencies, it increases drastically with frequency toward THz region. This means that broadband and high power amplification may be realized by an innovative device design in the millimeter wave and sub-millimeter wave regions where power level of conventional semiconductor devices fall very rapidly with the increase of frequency. A large modulation of conductance due to interactions between surface plasma waves of 2DEG carriers in AlGaAs/GaAs hetero-structure and electromagnetic space harmonic slow waves was observed experimentally although no net negative conductance was observed due to non-uniformity of field distribution under interdigital gates. Net negative conductance can be obtained if a uniform field distribution can be realized. The result seems to prove the existence of surface plasma wave interactions even under the strongly collision dominant situation in the microwave region and provides great hope for increased interactions at THz frequencies with nearly collision free conditions. The uniformity of field distribution was improved by applying a dc segmented rf coupled slow-wave structure instead of dc connected structure. In our present design, the fingers at the edge of channel were connected directly to the main gate electrodes. The pinch off of current can be delayed at higher voltage if the fingers at the edge of channel are totally isolated from the main gate electrodes. We believe

that the pinch-off characteristics in our present designed device are resulted from this matter.

ACKNOWLEDGMENTS

The author (A.M.Hashim) would like to thank Professor S. Kasai, Professor T. Hashizume and Professor H. Hasegawa for fruitful discussion and guidance on theoretical and experimental work. This work was partly supported by Japan's Ministry of Education, Culture and Technology (MEXT), Malaysia's Ministry of Science, Technology and Innovation (MOSTI) and Malaysia's Ministry of Higher Education (MOHE) through 21st century COE Program Meme-media Technology Approach to the RandD of Next Generation ITs, Science Fund Vote 79174 (03-01-06-SF0283) and Fundamental Research Grant Scheme Vote 78205 and 78417, respectively. The author also would like to thank Research Center for Integrated Quantum Electronics, Hokkaido University and Institute of Ibnu Sina, Universiti Teknologi Malaysia for fabrication facilities.

REFERENCES

Baudrand, H., D. Lilonga and T.E. Khoury, 1984. Amplification by interdigital excitation of space-charge waves in semiconductors. IEEE Trans. Microwave Theory Tech., 32: 1434-1441.

Chamberlain, J.M. and R.E. Miles, 1997. New Directions in Terahertz Technology. 1st Edn., Springer, USA., ISBN-10: 0792345371. pp: 444.

Coldren, L.A. and G.S Kino, 1974. The InSb on a piezoelectric Rayleigh wave amplifier. IEEE Trans. Electron Devices, 21: 421-427.

Dyakonov, M. and M.S. Shur, 1993. Shallow water analogy for a ballistic field effect transistor: New Mechanism at plasma wave generation by dc current. Phys. Rev. Lett., 71: 2465-2468.

Ettenberg, M. and J.S. Nadan, 1970. The theory of the interaction of drifting carriers in a semiconductor with external traveling-wave circuits. IEEE Trans. Electron Devices, 17: 219-223.

Freeman, J.C., V.L. Newhouse and R.L. Gunshor, 1973. Interactions between slow circuit waves and drifting carriers in InSb and Ge at 4.2 K. Applied Phys. Lett., 22: 641-643.

Hasegawa, H., M. Furukawa and H. Yanai, 1971. Properties of microstrip line on Si-SiO/sub 2/ system. IEEE Trans. Microwave Theory Tech., 19: 869-881.

Hashim, A.M., T. Hashizume, K. Iizuka and H. Hasegawa, 2003. Plasma wave interactions in microwave to THz range between carriers in semiconductor 2DEG and interdigital slow waves. Superlattices Microstruct., 34: 531-537.

Hashim, A.M., S. Kasai, T. Hashizume and H. Hasegawa, 2005. Large modulation of conductance in interdigital-gated HEMT device due to surface plasma wave interactions. Jap. J. Applied Phys., 44: 2729-2734.

Hashim, A.M., 2006. Plasma waves in semiconductors and their interactions with electromagnetic waves up to THz region. Ph.D. Thesis, Hokkaido University.

Hashim, A.M., S. Kasai, T. Hashizume and H. Hasegawa, 2007a. Integration of interdigital-gated plasma wave device for proximity communication system application. Microelectronics J., 38: 1263-1267.

Hashim, A.M., S. Kasai, T. Hashizume and H. Hasegawa, 2007b. Novel structure of GaAs-based interdigital-gated HEMT devices for solid-state THz wave amplifier. Microelectronics J., 38: 1268-1272.

Hashim, A.M., S. Kasai and H. Hasegawa, 2008. Observation of first and third harmonic responses in two-dimensional AlGaAs/GaAs HEMT devices due to plasma wave interaction. Superlattices Microstruct., 44: 754-760.

Iizuka, K., A.M.B. Hashim and H. Hasegawa, 2004. Surface plasma wave interactions between semiconductor and electromagnetic space harmonics from microwave to Thz range. Thin Solid Films, 464-465: 464-468.

Miles, R.E., P. Harison and D. Lippens, 2001. Terahertz Sources and Systems. 1st Edn., Kluwer Academic Publishers, Boston, ISBN: 0792370961.

Mustafa, F. and A.M. Hashim, 2010. Generalized 3D transverse magnetic mode method for analysis of interaction between drifting plasma waves in 2DEG-structured semiconductors and electromagnetic space harmonic waves. Prog. Electromagn. Res., 102: 315-335.

Robinson, B.B. and G.A. Swartz, 1967. Two-stream instability in semiconductor plasmas. J. Applied Phys., 38: 2461-2465.

Seki, S. and H. Hasegawa, 1984. Analysis of crosstalk in very high-speed LSI/VLSI's using a coupled multiconductor MIS microstrip line model. IEEE Trans. MTT., 32: 1715-1720.

Shur, M.S., L. Jian-Qiang and M.I. Dyakonov, 1999. Terahertz applications of plasma wave electronics. IEEE MTT-S Int., 3: 937-940.

Silvester, P., 1968. TEM wave properties of microstrip transmission lines. Proc. IEEE., 115: 43-48.

Solymar, L. and E. Ash, 1966. Some traveling-wave interactions in semiconductor theory and design considerations. Int. J. Electronics, 20: 127-148.

Sumi, M., 1967. Traveling-wave amplification by drifting carriers in semiconductors. Jap. J. Applied Phys., 6: 688-698.

Sumi, M. and T. Suzuki, 1968. Evidence for directional coupling between semiconductor carriers and slow circuit waves. Applied Phys. Lett., 13: 326-327.

Swanenburg, T.J.B., 1973. Negative conductance of an interdigital electrode structure on a semiconductor surface. IEEE Trans. Electron Devices, 20: 630-637.

Thiennot, J., 1972a. Space charge waves in semiconductors and progressive amplification in the solid state. J. Phys., 33: 219-228.

Thiennot, J., 1972b. The effect of the surface electric charge on the gain of a solid state traveling wave amplifier. J. Phys., 33: 781-786.

Thompson, J.J., M.R.S. Taylor, A.M. Thompson, S.P. Beaumont and N. Apsley, 1991. Gallium arsenide solid state traveling wave amplifier at 8 GHz. Electronics Lett., 27: 516-518.

Vural, B. and M. Steele, 1969. Wave Interactions in Solid State Plasmas. McGraw-Hill, New York.

Watanabe, I., K. Shinohara, T. Kitada, S. Shimomura and A. Endoh *et al*., 2007. Effect of heterointerface flatmess on device performance of InP-based high electron mobility transistor. Jap. J. Applied Phys., 46: 2325-2329.

Zotter, B., 1968. Traveling wave amplification by drifting carriers in semiconductors. U.S. Army ECOM Rep., 2958: 40-40.